Soft Matter



PAPER View Article Online



Water ring-bouncing on repellent singularities†

Cite this: DOI: 10.1039/c7sm02004

Pierre Chantelot, ab Ali Mazloomi Moqaddam, Anaïs Gauthier, bhyam S. Chikatamarla, Christophe Clanet, bhyam S. Chi

Received 8th October 2017, Accepted 8th January 2018

DOI: 10.1039/c7sm02004j

rsc.li/soft-matter-journal

Texturing a flat superhydrophobic substrate with point-like superhydrophobic macrotextures of the same repellency makes impacting water droplets take off as rings, which leads to shorter bouncing times than on a flat substrate. We investigate the contact time reduction on such elementary macrotextures through experiment and simulations. We understand the observations by decomposing the impacting drop reshaped by the defect into sub-units (or blobs) whose size is fixed by the liquid ring width. We test the blob picture by looking at the reduction of contact time for off-centered impacts and for impacts in grooves that produce liquid ribbons where the blob size is fixed by the width of the channel.

Introduction

The most spectacular property of superhydrophobic materials might be their ability to reflect impacting drops. 1-4 This property is important for applications because it defines an anti-rain function that preserves the dryness of a solid in wet weather⁵ and prevents impregnation,6 wetting,7,8 optical distortion9 and corrosion¹⁰ arising from contact with water. When wettability is low enough, the spreading of impinging drops is followed by recoil and takeoff, in a spring-like fashion.² Consequently, the contact time τ of the rebound is set by the (square root of the) ratio between mass (representing inertia) and surface tension (standing for spring stiffness) so that the contact time scales as $\sqrt{\rho R^3/\gamma}$ where ρ and γ stand for the density and surface tension of water, and R is the drop radius. This time is on the order of 10 ms for millimeter-size drops, which can be large enough to induce freezing when the solid is very cold. 3,11,12 Hence it is relevant to find ways to reduce the time τ , 3,4,14-16 which also favors repellency of water containing surfactants. 13 As shown recently,^{3,4} a reduction of the contact time can be triggered by placing macrotextures such as ridges or cones at the solid surface. The scale of these textures is intermediate between the drop size and that of nano/microstructures needed for repellency, which reshapes the liquid at impact and consequently tunes the contact time. Here we propose to test this idea with the simplest imaginable macrotexture, that is, a mere point-like defect. Despite its extreme simplicity, this texture is found to

Contact time reduction on repellent singularities

The substrate we consider is obtained by attaching a glass bead with radius $r=200\pm20~\mu m$ to a silicon wafer. The bead is deposited on the center of $\sim 100~\rm pL$ of glue brought with a thin fiber, so that the glue meniscus remains small and axisymmetric. After drying, the flat surface and the bead are made equally water-repellent by spraying a solution of hydrophobic nanobeads (with size $\sim 20~\rm nm$) dispersed in acetone (Ultra Ever Dry, UltraTech International). Once the solvent is evaporated, the solid is coated by nanobeads that form aggregates with a characteristic size of 500 nm (see Fig. S1, ESI†), which makes it uniformly super hydrophobic. Water laid on the textured surface exhibits advancing and receding contact angles of $166^{\circ} \pm 4^{\circ}$ and $159^{\circ} \pm 2^{\circ}$, respectively. These high angles and low hysteresis are typical of water-repellent materials.

Our experiment consists in impacting distilled water (density $\rho = 1000 \text{ kg m}^{-3}$ and surface tension $\gamma = 72 \text{ mN m}^{-1}$) on these macro/nano-textured substrates. As sketched in Fig. 1a, we first perform centered impacts. The drop radius R can be varied between 1 and 2.4 mm by using calibrated needles, whose height is adjusted to generate impact speeds V between 0.4 and 1.6 m s⁻¹. At such velocities, the integrity of drops is always preserved. Top and side views are shot using two high-speed video cameras (Phantom V7) working at typically 10 000 frames per second. The drop oscillations can be estimated from the experimental movies: as they always remain smaller than 17%

induce reduction of the contact time comparable to that of more extended structures (such as lines) and, surprisingly, to maintain this reduction as impacts get off-centered – a property of obvious practical interest if we think of anti-rain features.

^a Physique & Mécanique des Milieux Hétérogènes, UMR 7636 du CNRS, ESPCI, 75005 Paris, France

^b LadHyX, UMR 7646 du CNRS, École polytechnique, 91128 Palaiseau, France

^cAerothermochemistry and Combustion Systems Laboratory, Mechanical and Process Engineering Department, ETH Zurich, 8092 Zurich, Switzerland

 $[\]dagger$ Electronic supplementary information (ESI) available. See DOI: 10.1039/c7sm02004j

Paper Soft Matter

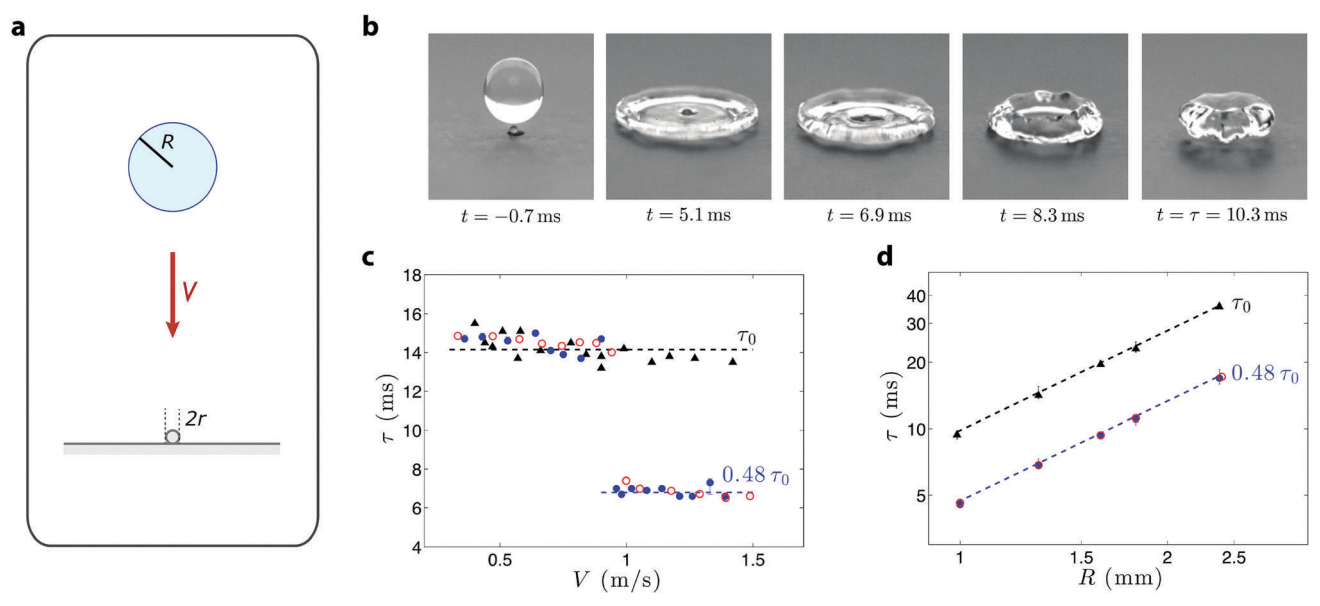


Fig. 1 (a) A water drop with radius R (between 1 and 2.4 mm) impacts at a velocity V (between 0.4 and 1.6 m s⁻¹) a glass bead with radius $r = 200 \,\mu\text{m}$ glued to a silicon wafer. Both the substrate and the bead are made equally superhydrophobic. (b) High-angle shot of a water droplet with radius R = 1.6 mm impacting the point-like defect at V = 1.2 m s⁻¹ (centered impact). The drop takes off as a ring at a time $\tau = 10.3$ ms. (c) Contact time τ of water drops (R = 1.3 mm) bouncing off a repellent wafer (black triangles, τ_0) and a similar surface with the defect (blue dots, experimental data; red circles, simulation results). Both times are plotted as a function of the impact velocity V. (d) Contact times τ (with defect) and τ_0 (without defect) as a function of the drop radius R. τ is measured in the high-speed regime ($V > V^*$) where it is reduced (blue dots, experimental data; red circles, simulation results). Fits are $au_0 \approx 2.6 (\rho R^3/\gamma)^{1/2}$ (black dashed line) and $au \approx 0.48 au_0$ (blue dashed line); error bars stand for the variations seen in the two plateaus in (c), which partially originate from the oscillations of the falling drop.

of the drop radius, they do not disturb significantly the outcome of impacts - and specifically hardly affect the measurement of the contact time.

Drops always fully bounce on the substrate albeit with two distinctly different behaviors. (1) At a low impact velocity $(V < 0.9 \text{ m s}^{-1} \text{ for } R = 1.3 \text{ mm})$, the rebound is not affected by the macrotexture. Water spreads, recoils and takes off as it does when impacting a flat superhydrophobic material. (2) For $V > V^*$ ($V^* = 0.9 \text{ m s}^{-1}$ for R = 1.3 mm), the drop adopts an unusual ring shape as it leaves the substrate (Fig. 1b and Supplementary Movie 1, ESI†). The defect does not modify the extension of the spreading drop, but the thin central film gets punctured. This film dewets outwards until it collides with the outer receding rim moving in the opposite direction. The collision creates an upward motion, which eventually leads to the takeoff of a ring. This ring then closes, which generates oscillations without fragmenting water, provided the Weber number We = $\rho RV^2/\gamma$ remains smaller than 40.

The contact time τ is measured between the drop/macrobead first contact and take off from the repellent material, including the macrotexture. τ reflects the two regimes of impact, as visible in Fig. 1c. As reported earlier² and confirmed in Fig. 1c, its value τ_0 on a flat repellent substrate (black triangles) does not depend on impact velocity. In contrast, two plateaus are observed in the presence of the point-like macrotexture (blue dots in Fig. 1c). While we have $\tau \approx \tau_0$ for $V < V^*$, the contact time is drastically and abruptly reduced for $V > V^* = 0.9 \text{ m s}^{-1}$, where it is found to reach a new value $\tau \approx 0.48 \tau_0$ in a large range of velocities. This reduction of contact time univocally corresponds to the cases

when water takes off with a ring-shape. The transition is caused by the puncture of the film, which occurs when the size of the defect is close to the film thickness *h*, set by the Weber number. For a spherical defect with radius $r = 200 \mu m$ the transition occurs for We = 20 ± 2 (as indicated in Fig. S2, ESI†). In the regime $V > V^*$ (Fig. 1d, same symbols as in Fig. 1c), both τ_0 and τ are measured as a function of the drop radius R. For each family of data, $\tau(R)$ follows a scaling law of exponent 1.50 \pm 0.03. Hence contact times are proportional to the square root of the drop mass, a signature of the balance between inertia and capillarity.^{2,3} On a flat surface,³ this balance can be written $\tau_0 \approx 2.6 \ (\rho R^3/\gamma)^{1/2}$, a law drawn with a black dashed line in Fig. 1c and d. In the presence of the point-like defect, the scaling law above V* is the same $(\tau \sim (\rho R^3/\gamma)^{1/2})$, yet with a prefactor of 1.24 ± 0.3 instead of 2.60 ± 0.2 .

Our aim is to understand how a marked reduction of the contact time can arise from the presence of a point-like, isotropic, hydrophobic defect. A first approach consists of simulating the complex interaction of water with the substrate. To that end, we use the entropic lattice Boltzmann method (ELBM) for multiphase flows. 17-19 The simulation parameters are matched to the experimental conditions by identifying the Weber number and the Reynolds number (Re = $\rho RV/\eta$, where η is the liquid viscosity), and considering a solid-liquid contact angle of 161° comparable to that of our surfaces. To convert lattice time $t_{\rm LB}$ into seconds, we first compute the inertio-capillary time $T_{LB} = (\rho R^3/\gamma)^{1/2}$ using the density, droplet radius and surface tension in lattice units. Next, inertio-capillary time T_{exp} is extracted from the experimental data and the reduced times for both the

Soft Matter Paper

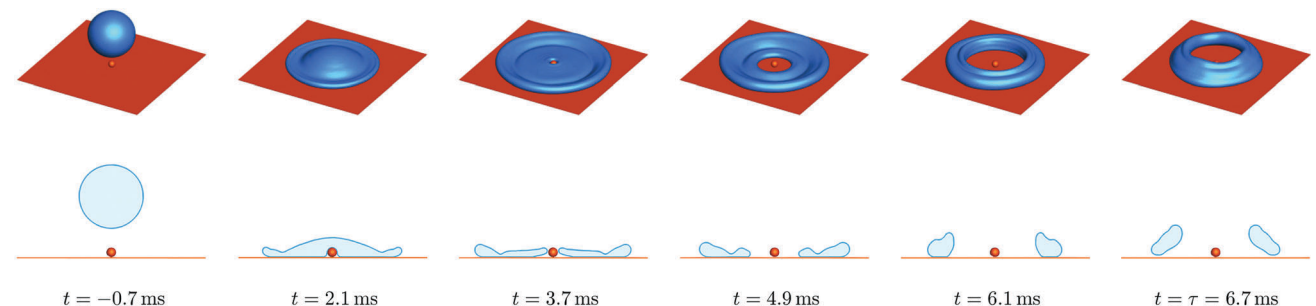


Fig. 2 Simulation of a droplet with radius R = 1.3 mm impacting at V = 1.28 m s⁻¹ a substrate macrotextured by a sphere with radius r = 200 μ m. For each time, we show high-angle views and cross-sections, allowing us to access the formation of the ring (at t = 3.7 ms), the collision between opposite rims (at t = 6.1 ms) and the takeoff (at t = 6.7 ms)

experiment and the simulation are matched, $t_{LB}/T_{LB} = t/T_{exp}$. Thus, given t_{LB} (the number of time steps), we uniquely obtain the corresponding physical time $t = (T_{\text{exp}}/T_{\text{LB}})t_{\text{LB}}$. Fig. 2 and Supplementary Movie 2 (ESI†) show ELBM simulation of the drop impact on a spherical macrodefect at Weber number We \sim 30, corresponding to the conditions explored in Fig. 1c. The sequence is observed to be in excellent agreement with experiments: the drop spreads and thins out before a ring forms and departs at a time τ = 6.7 ms, a value close to measurements ($\tau = 6.6 \pm 0.1$ ms). Simulations also allow us to explore the quantities more difficult to access experimentally. Specifically, Fig. 2 shows the evolution of the drop cross-section during impact (hidden by a peripheral rim in the experiments). Original observations can be made: (i) central dewetting occurs when the film thickness compares to the size of the defect that acts as a nucleator of dewetting. For a given drop, this fixes the Weber number at which a ring forms. (ii) Vertical momentum is brought to the system when the rim arising from the dewetting film collides with the receding peripheral outer rim. (iii) The outer bulge carries the dominant momentum so that the latter shock is not symmetric. This generates obliquity in the crosssection of the departing ring, in the final view in Fig. 2. Further information regarding the flow inside the drop can be seen in the Supplementary Movie 3 (ESI†), and it confirms that collision between opposing rims is the mechanism for creating upward momentum. All these observations do not depend on the actual shape of the surface defect, as shown in Fig. S1 in the ESI† where we show the experimental results for conical hills and cylindrical defects. We can finally extract from simulations the contact time as a function of V and R. Simulation results in Fig. 1c and d (empty red circles) reproduce the two plateaus corresponding to the two regimes of impact, in excellent quantitative agreement with experiments.

Blob model

Earlier studies showed that reshaping drops at impact generally affects their contact time. Water impinging slender defects (ridges and fibers) makes lobes that spread and retract, so that it was proposed to take the lobe mass m (instead of the drop one, m_0) as the one fixing the contact time, ¹⁴ leading to a reduction of this time by a factor $(m_0/m)^{1/2}$. Here we propose to generalize this idea to situations where there are no distinct lobes, such as observed when water takes off with a ring shape. Then we consider impacts in grooves, so that impinging water is channeled and impact geometry anisotropic, allowing us to test our model in very different situations.

A drop on a point-like defect successively spreads and retracts, but the retraction stage occurs both from the drop edges and center, if the defect is large enough to pierce the spreading film. Hence the ring width ℓ appears to be the relevant distance characterizing liquid sub-units (or blobs): for each of these blobs (with mass m), water spreads and later recoils, a condition for using the spring-like model. From the corresponding law for the contact time, we expect the contact time τ to scale as $(m/\gamma)^{1/2}$, so that τ can be deduced from τ_0 by a direct comparison between the blob and drop volumes. As sketched in Fig. 3a, the blob size ℓ compares to the maximum radius of spreading R_{max} , provided that $r \ll R_{\rm max}$ (a condition fulfilled in our study). For centered impacts, the impact pattern is axisymmetric, so that the blobs composing the drop have a common contact time τ . Assuming that the average height h of the spread liquid is not affected by the presence of the point-like defect, the ratio between blob and drop volumes is estimated as the drop reaches its maximum spreading as $\pi \ell^2 h / 4\pi R_{\text{max}}^2 h$, that is, $\sim 1/4$. This immediately yields $\tau \approx \tau_0/2$, in good agreement with our data where we have $\tau \approx 0.48\tau_0$ (Fig. 1c and d).

A first way to test the blob model consists of off-centering the drops, which tunes the blob mass m (Fig. 3b). Off-centering is achieved by adjusting the position of the syringe from which drops are dispensed. The use of micrometric screws allows us to select the distance x between the drop center and the defect center with a precision of 20 µm. For a given off-centering distance x > 0, blobs do not have anymore a unique size ℓ , that instead spans between a minimum $\ell_- < R_{\rm max}$ and a maximum $\ell_+ > R_{\rm max}$ on opposite sides of the defect (Fig. 3b). As observed in Fig. 3c (with x = 0.7 mm and V = 1.3 m s⁻¹ > V*), asymmetrical impacts generate asymmetrical rebounds. Spreading and hole formation in the film are similar to what we reported earlier, but the drop does not anymore take off in just one time: the blob with size ℓ_{-} gets lifted after 5.7 ms, while the largest blob with size ℓ_{+} departs 1.7 ms later, which fixes the contact time τ of the whole drop – found to be 7.4 \pm 0.1 ms here. Simulated cross-sections



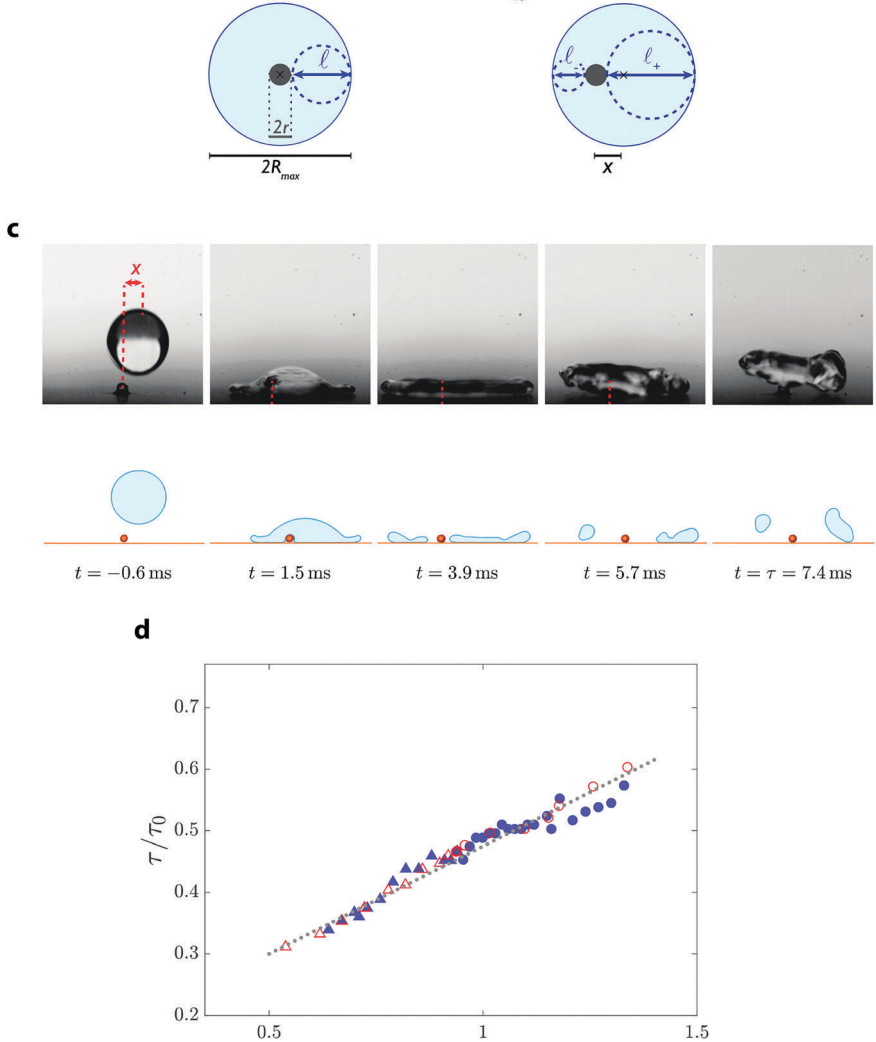


Fig. 3 (a) Top sketch of a drop as it reaches its maximum radius after impacting a point-like defect (in black). Impact is centered, and we denote as ℓ the width of the ring. (b) Similar sketch for an impact off-centered by a distance x. The blobs (marked with dotted lines) are now asymmetric, with minimum and maximum size ℓ_- and ℓ_+ . (c) Water droplet (R=1.3 mm) impacting at V=1.3 m s⁻¹ a bead with diameter r=200 µm, with off-centering x=0.7 mm. The left and right parts depart after 5.7 ms and $\tau\approx7.4$ ms, respectively. The corresponding simulations quantitatively match the experiments. (d) Contact time τ normalized by τ_0 as a function of the normalized blob size ℓ/R_{max} . Dots are experimental data and red circles simulations for the largest blob (size ℓ_+). Triangles correspond to the departure of the smallest blob (size ℓ_-).

 ℓ/R_{max}

displayed in the same figure quantitatively confirm this description. Despite a strong off-centering (x/R ≈ 0.55), contact time remains markedly reduced ($\tau \approx 0.52\tau_0$), and even comparable to that for centered impacts ($\tau \approx 0.48\tau_0$). At $t>\tau$, the rising non-axisymmetric ring is tilted (see also Supplementary Movies 4 and 5, ESI†), owing to the early takeoff of the narrow side of the ring.

Based on side views and cross-sections at impact (Fig. 3e), we can extract two contact times that respectively correspond to blob sizes ℓ_- and ℓ_+ . We report in Fig. 3d all the pairs of contact times obtained after varying x from 0 to R, the maximum off-centering for which we still observe ring bouncing. τ is normalized by τ_0 , and it is plotted as a function of the blob size ℓ normalized by $R_{\rm max}$, a fixed distance since we set the impact velocity ($V = 1.3 \, {\rm m \, s^{-1}} > V^*$) and the drop size ($R = 1.3 \, {\rm mm}$).

Contact times for "small" ($\ell/R_{\rm max} < 1$) and "large" blobs ($\ell/R_{\rm max} > 1$) are respectively reported with triangles and circles. In addition, we indicate with empty symbols the values obtained from simulations and found here again to nicely agree with data. The contact time τ in Fig. 3d increases regularly with the blob size ℓ , and the variation is close to be linear (dotted line). This observation allows us to test the blob model. Assuming that we have $m/m_0 \approx \pi \ell^2/4\pi R_{\rm max}^2$, and applying the spring scaling $\tau \sim (m/\gamma)^{1/2}$, we obtain $\tau \approx \tau_0 (\ell/2R_{\rm max})$, that is, a linear relationship between τ and ℓ , as observed experimentally. Scaling the contact time τ and blob size ℓ by τ_0 and $R_{\rm max}$, respectively, we expect from the model a coefficient of proportionality 1/2. The fit drawn with a dotted line in Fig. 3d has a slope of 0.37. This discrepancy may arise from the estimation of the blob

Soft Matter

volume. By assuming that the spread drop has a constant thickness h, we do not take into account the peripheral rim (visible in Fig. 1b), which leads us to underestimate the volume of small blobs and overestimate that of big blobs. Then we expect a prefactor smaller than the predicted value of 1/2, as seen in experiments and simulations.

Off-centering thus allows us to tune the blob size in a continuous manner, and to measure the contact times associated with asymmetric blobs. We found that even an off-centering of order the drop radius R induces a large reduction of the contact time, a result of obvious practical interest. Rain randomly hits solids, so that it is valuable to keep an effect for x as large as R, and even above as shown in Fig. S2 of the ESI.† The blob picture provides an interpretation for this property, and we can be surprised by the efficiency of such a simple argument; hence the idea to test the model in a different geometry.

Finally, we test the blob picture in a situation when the blob size is dictated by the substrate geometry. A groove etched in a solid substrate will force an impacting liquid to elongate, which results in an anisotropic impact with a fixed width - that of the groove, denoted as W. This experiment is sketched in Fig. 4a, and it can be seen as akin to ring bouncing, if considering a ribbon as an unfolded torus. We machine a groove in brass,

with depth 0.5 mm and width W = 2.2 mm. Owing to the presence of sharp edges, water impacting such a repellent groove pins along the edges, which artificially modifies and/or scatters the contact time. Hence we choose here to work in the Leidenfrost situation, obtained without treatment of the brass and after heating it at a temperature of 350 °C – which also generates rebounds similar to that observed on a repellent material at room temperature. We use ethanol as liquid, with $\rho = 728 \text{ kg m}^{-3}$ and γ = 17.4 mN m⁻¹ at the boiling point 78 °C at standard pressure.

Fig. 4b shows simultaneous top and side views of a drop with radius R = 0.93 mm hitting a groove at V = 0.7 m s⁻¹. The liquid is channeled by the groove so that it elongates at fixed width W, until it reaches a maximum l_{max} (at t = 3.2 ms in Fig. 4b). Then the bulges at the walls retract (so that the drop further elongates with a smaller width) and collide, which leads to the takeoff of a liquid cylinder at τ = 7.2 \pm 0.1 ms, a time shorter than τ_0 = 13.6 \pm 1 ms for Leidenfrost drops on a flat plate. In Fig. 4c, we report the contact times τ_0 (triangles) and τ (circles) as a function of the impact velocity V. Contrasting with the time τ_0 , τ decreases with V and it is always reduced compared to τ_0 , by a factor that can be typically of order 2.

We choose the blob size as the groove width, since all these sub-units composing the elongated drop successively spread

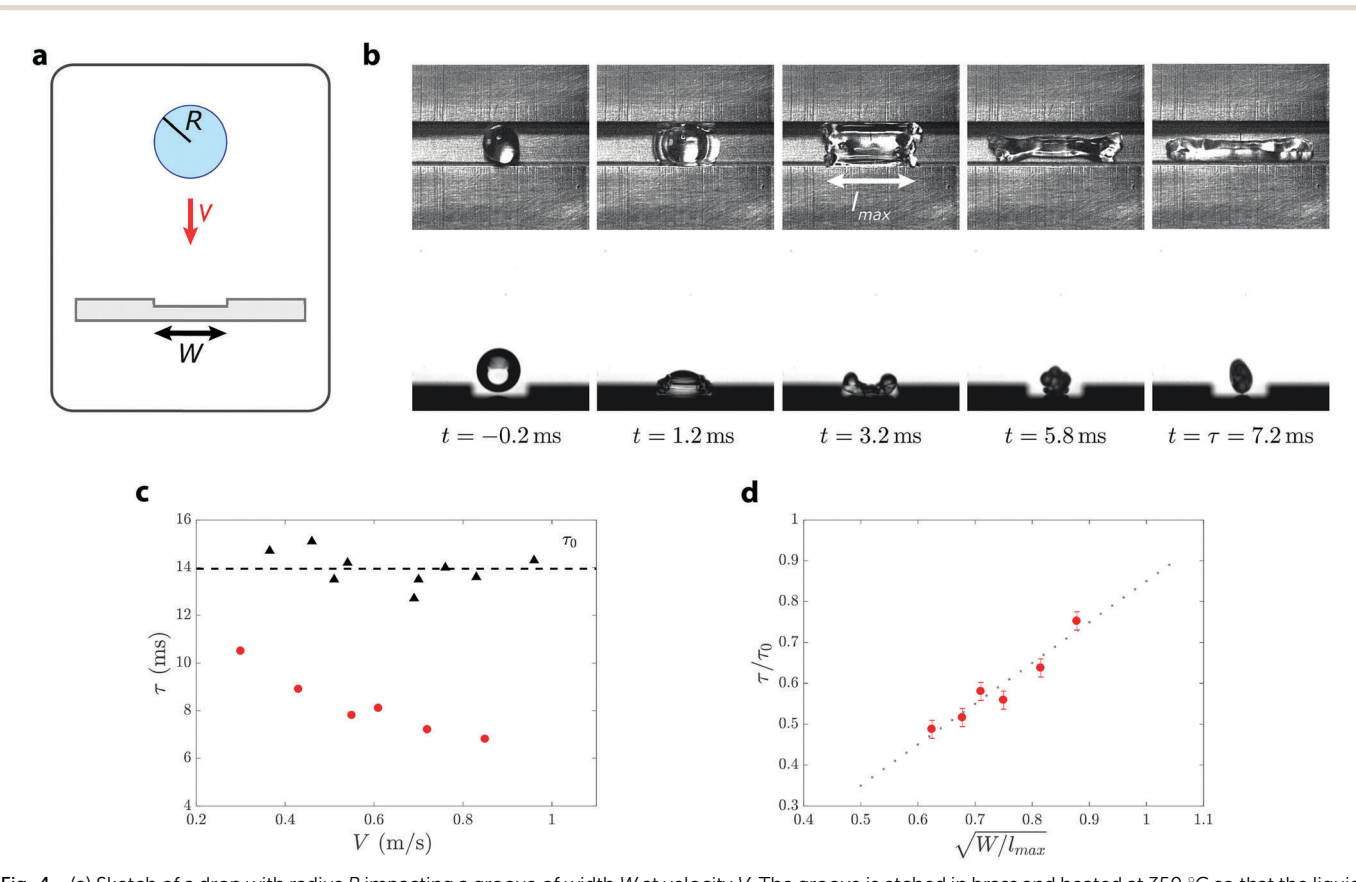


Fig. 4 (a) Sketch of a drop with radius R impacting a groove of width W at velocity V. The groove is etched in brass and heated at 350 °C so that the liquid is in the Leidenfrost state. (b) Top and side views of an ethanol drop (R = 0.93 mm and $V = 0.7 \text{ m s}^{-1}$) impacting a groove of width W = 2.2 mm. The droplet reaches a maximal extension l_{max} and it bounces as a cylinder after 7.2 ms, a time shorter than τ_0 , the contact time on a flat surface. (c) Contact time τ (circles) as a function of V for W = 2.2 mm: τ is always smaller than the contact time τ_0 of Leidenfrost drops on a flat surface (triangles). (d) Normalized contact time τ/τ_0 as a function of $(W/l_{max})^{1/2}$, for the data of Fig. 4c. The dotted line has a slope 1.

Paper Soft Matter

and recoil perpendicularly to the groove axis. The drop volume can be written $\Omega = Wl_{\text{max}}h$ (where h is the average ribbon thickness), while each blob has a volume $\omega = W^2h$. We expect τ/τ_0 to vary as $(\omega/\Omega)^{1/2}$, which yields $\tau = \tau_0(W/l_{\text{max}})^{1/2}$. Hence, we predict a scaling behavior between the normalized contact time and the inverse of the aspect ratio of the ribbon, as observed in Fig. 4d where we plot τ/τ_0 as a function of $(W/l_{\text{max}})^{1/2}$. The dotted line has a slope of 1.0 \pm 0.1, a factor close to one as expected from our model. More generally, the groove experiment shows that the blob picture is robust with respect to the change of geometry. The number of blobs $N = l_{\text{max}}/W$ was varied by tuning the impact velocity, which sets $l_{max}(V)$ and thus N. As a consequence, the contact time τ here decreases with the impact speed V, in sharp contrast with what we saw with a point-like defect for which the blob size changes proportionally to the spreading size.

Conclusion

Reshaping interfaces after impact most generally modifies to a large extent the contact time of bouncing drops. Water can be sculpted by placing at the solid surface macrotextures with a size intermediate between the drop radius and that of the hydrophobic microtextures. A first case discussed in the literature concerns structures that divide the impinging drop in n countable entities.^{3,14} Then the contact time is reduced by a factor of $n^{1/2}$, which can be understood using a spring-like model.14 Here we discuss how singular textures reshape impacting water without division, yet with a large reduction of the contact time. We propose a new tool for understanding this effect. Reshaping necessarily introduces one (or several) new characteristic size(s), on the scale of which we define liquid "blobs" that individually act as smaller drops possibly still connected to the other blobs. The contact time is that of the blob, and it is thus smaller than the time of bouncing determined in regular experiments. We could use our results in two kinds of situations: either blobs are monodisperse (centered impact on a dot, impact in a groove), in which case the contact time is fixed by the blob size; or they are polydisperse (off-centered impacts on dots), in which case the contact time is fixed by the size of the largest blob. In all these situations, our elementary approach was found to quantitatively capture the contact time reduction and behavior as a function of impact velocity observed in both simulations and experiments. In addition, the generality of the approach makes the blob picture relevant to understand cases where the reduction of contact time remains unexplained, such as the "sausage mode" of bouncing reported on curved materials,15 or to discuss new situations such as impact in assemblies of dots. Further research on this topic might also concentrate on the details of the impact on the blob scale, which might allow us to understand in a deeper way the relevance and the limits of our description.

Conflicts of interest

There are no conflicts to declare.

Soft Matter

Acknowledgements

We thank Direction Générale de l'Armement (DGA) for contributing to the financial support. IVK and SSC acknowledge support by ERC Advanced Grant 291094-ELBM and by SNF grant 200021_172640. AMM was supported by ETH grant ETH35-12-2. Computational resources at the Swiss National Super Computing Center CSCS were provided under the grant s492 and s630.

References

- 1 R. Blossey, Self-cleaning surfaces virtual realities, Nat. Mater., 2003, 2, 301-306.
- 2 D. Richard, C. Clanet and D. Quéré, Contact time of a bouncing drop, Nature, 2002, 417, 811.
- 3 J. C. Bird, R. Dhiman, H.-M. Kwon and K. K. Varanasi, Reducing the contact time of a bouncing drop, Nature, 2013, 503, 385-388.
- 4 Y. Liu, L. Moevius, X. Xu, T. Qian, J. M. Yeomans and Z. Wang, Pancake bouncing on superhydrophobic surfaces, Nat. Phys., 2014, 10, 515-519.
- 5 P. Roach, N. J. Shirtcliffe and M. I. Newton, Progress in superhydrophobic surface development, Soft Matter, 2008, 4, 224-240.
- 6 H. Ogihara, J. Xie, J. Okagaki and T. Saji, Simple method for preparing superhydrophobic paper: spray-deposited hydrophobic silica nanoparticle coatings exhibit high water-repellency and transparency, Langmuir, 2012, 28, 4605-4608.
- 7 X. Gao and L. Jiang, Biophysics: water-repellent legs of water striders, Nature, 2004, 432, 36.
- 8 K. M. Wisdom, J. A. Watson, X. Qu, F. Liu, G. S. Watson and C.-H. Chen, Self-cleaning of superhydrophobic surfaces by self- propelled jumping condensate, Proc. Natl. Acad. Sci. U. S. A., 2013, 110, 7992-7997.
- 9 X. Deng, L. Mammen, H. J. Butt and D. Vollmer, Candle soot as a template for a transparent robust superamphiphobic coating, Science, 2012, 335, 67-70.
- 10 J. Ma, X. Y. Zhang, D. P. Wang, D. Q. Zhao, D. W. Ding, K. Liu and W. H. Wang, Superhydrophobic metallic glass surface with superior mechanical stability and corrosion resistance, Appl. Phys. Lett., 2014, 104, 173701.
- 11 L. Mishchenko, B. Hatton, V. Bahadur, J. A. Taylor, T. Krupenkin and J. Aizenberg, Design of ice-free nanostructured surfaces based on repulsion of impacting water droplets, ACS Nano, 2010, 4, 7699-7707.
- 12 S. Jung, M. K. Tiwari, N. Vuong Doan and D. Poulikakos, Mechanism of supercooled droplet freezing on surfaces, Nat. Commun., 2012, 3, 615.
- 13 M. Song, J. Ju, S. Luo, Y. Han, Z. Dong, Y. Wang, Z. Gu, L. Zhang, R. Hao and L. Jiang, Controlling liquid splash on superhydrophobic surfaces by a vesicle surfactant, Sci. Adv., 2017, 3, e1602188.
- 14 A. Gauthier, S. Symon, C. Clanet and D. Quéré, Water impacting on superhydrophobic macrotextures, Nat. Commun., 2015, 6, 8001.
- 15 Y. Liu, M. Andrew, J. Li, J. M. Yeomans and Z. Wang, Symmetry breaking in drop bouncing on curved surfaces, Nat. Commun., 2015, 6, 10034.

16 Y. Liu and Z. Wang, Superhydrophobic porous networks for enhanced droplet shedding, Sci. Rep., 2016, 6, 33817.

Soft Matter

- 17 A. Mazloomi, S. S. Chikatamarla and I. V. Karlin, Entropic lattice Boltzmann method for multiphase flows, Phys. Rev. Lett., 2015, 114, 174502.
- 18 A. Mazloomi, S. S. Chikatamarla and I. V. Karlin, Entropic lattice Boltzmann method for multiphase flows: fluid-solid
- interfaces, Phys. Rev. E: Stat., Nonlinear, Soft Matter Phys., 2015, 92, 023308.
- 19 A. Mazloomi, S. S. Chikatamarla and I. V. Karlin, Simulation of binary droplet collisions with the entropic lattice Boltzmann method, Phys. Fluids, 2016, 28, 022106.
- 20 M. Kunihide and M. Itaru, The behavior of a water droplet on heated surfaces, Int. J. Heat Mass Transfer, 1984, 27, 781-791.